

Tuning spin-orbit coupling in the Kondo insulator $\text{Ce}_3\text{Bi}_4\text{Pt}_3$ by Pd substitution

S. Dzsaber¹, L. Prochaska¹, A. Sidorenko¹, G. Eguchi¹,
R. Svagera¹, M. Waas¹, A. Prokofiev¹, Q. Si², and S. Paschen^{1,2,*}

¹*Institute of Solid State Physics, Vienna University of Technology,
Wiedner Hauptstr. 8-10, 1040 Vienna, Austria and*

²*Department of Physics and Astronomy, Rice University, Houston, Texas 77005, USA**

(Dated: October 10, 2018)

Recent theoretical studies of topologically nontrivial electronic states in Kondo insulators have pointed to the importance of spin-orbit coupling (SOC) for stabilizing these states. However, systematic experimental studies that tune the SOC in Kondo insulators remain elusive. The main reason is that variations of (chemical) pressure or doping strongly influence the Kondo coupling J_K and the chemical potential μ – both essential parameters determining the ground state of the material – and thus possible SOC tuning effects have remained unnoticed. Here we present the successful growth of the substitution series $\text{Ce}_3\text{Bi}_4(\text{Pt}_{1-x}\text{Pd}_x)_3$ ($0 \leq x \leq 1$) of the archetypal (non-centrosymmetric) Kondo insulator $\text{Ce}_3\text{Bi}_4\text{Pt}_3$. The Pt-Pd substitution is isostructural, isoelectronic, and isosize, and therefore likely to leave J_K and μ essentially unchanged. By contrast, the large mass difference between Pt and Pd leads to a large difference in SOC, which thus is the dominating tuning parameter in the series. Surprisingly, with increasing Pd substitution level x , we observe a systematic closing of the Kondo insulator gap and a decrease of the characteristic energy below which magnetic moments are screened, demonstrating an unprecedented drastic influence of the SOC. The fully substituted end compound $\text{Ce}_3\text{Bi}_4\text{Pd}_3$ is a strongly correlated semimetal that shows indications of linear electronic dispersion with low quasiparticle velocity, as expected for a recently predicted Weyl-Kondo semimetal.

Topological phases [1] in condensed matter systems [2, 3], most recently encompassing also gapless variants [4], continue to attract great attention. To date, work has mostly focused on weakly correlated materials, but it is clear that yet more exotic physics awaits to be discovered in strongly correlated settings. Thus, the proposal that Kondo insulators [5, 6] exhibit topologically nontrivial metallic surface states [7, 8] was taken up enthusiastically and triggered many experimental studies, most notably on SmB_6 [9]. A key ingredient for a topologically nontrivial electronic structure in Kondo insulators is the strong spin-orbit coupling (SOC) of the heavy lanthanide $4f$ elements [7, 8], but the importance of SOC of the conduction electrons that hybridize with the $4f$ electrons has also been demonstrated [10]. In studies of the periodic Anderson model, the latter was shown to tune between different phases, including topological and topologically trivial Kondo insulators [10], Dirac-Kondo semimetals [11], and most recently Weyl-Kondo semimetals [12]. To link such studies directly to experiment it would be highly desirable to find an experimental “tuning knob” for SOC in Kondo systems. The availability of parameters that tune the Kondo interaction strength has been vital to the field of heavy fermion quantum criticality [13–15]. Here we demonstrate for the first time SOC tuning in a Kondo insulator.

Kondo insulators are materials where the Kondo interaction between localized $4f$ (and less frequently $5f$ or $3d$) electrons and itinerant s , p , and d electrons opens a narrow gap – of the order of 10 meV – in the electronic

density of states at the Fermi level [5, 6]. Among the archetypal cubic Kondo insulators that have been studied for decades (e.g., SmB_6 [16, 17], YbB_{12} [18, 19], FeSi [20, 21], $\text{Ce}_3\text{Bi}_4\text{Pt}_3$ [22–25]), $\text{Ce}_3\text{Bi}_4\text{Pt}_3$ appears as ideal starting material for our study. As Ce-based system it represents the conceptually simple situation of a single $4f$ electron as localized species. Its Kondo insulating ground state is well established [6, 22] and quite robust: The Kondo insulator gap persists up to 145 kbar [26] and is closed only for magnetic fields as high as 40 T [25]. $\text{Ce}_3\text{Bi}_4\text{Pt}_3$ lacks inversion symmetry in all three atomic (Ce, Bi, Pt) sublattices. Theoretical studies have suggested that $\text{Ce}_3\text{Bi}_4\text{Pt}_3$ hosts a topologically nontrivial band structure [7, 27].

Generally, chemical substitution with atoms of sizeable mass difference seems a promising route for SOC tuning because the atomic number Z (or the mass) enters the SOC parameter as $\lambda_{SOC} \sim Z^4$ [28]. In Kondo insulators, however, a clever choice of the type of substitution has to be made. A substitution of the $4f$ element (Ce) breaks the translational symmetry of the local moment sublattice, which leads to a loss of Kondo coherence. To keep the Kondo lattice intact, substitutions should therefore be limited to the nonmagnetic elements (Bi and Pt). The second constraint is that Kondo insulators, just as heavy fermion metals, react sensitively to even small changes of chemical pressure. Thus, to keep the Kondo coupling (J_K) tuning minimal, isosize substitutions should be used. Finally, Kondo insulators being insulators naturally makes them react strongly to changes in electron count and thus in the chemical potential (μ), which favours isoelectronic substitutions (without carrier “doping”).

* Corresponding author: pachen@ifp.tuwien.ac.at

Previous studies have failed to separate these different effects. For instance, in the Kondo semimetal CeNiSn, isoelectronic but non-isosize substitutions of Ni by Pt or Pd close the Kondo (pseudo)gap as a consequence of the increased unit cell volume and hence the decreased hybridization or Kondo coupling J_K [29, 30]. In $\text{Ce}_3\text{Sb}_4\text{Pt}_3$, the non-isosize and non-isoelectronic substitutions of Pt with Cu and Au both suppress the Kondo insulating state although Cu doping results in a reduced [31] and Au doping in an increased unit cell volume [32]. Thus, here the change in chemical potential appears to dominate.

Surprisingly, no substitution series of $\text{Ce}_3\text{Bi}_4\text{Pt}_3$ other than Ce-La replacements [33, 34] have yet been studied. Here we present first results on the series $\text{Ce}_3\text{Bi}_4(\text{Pt}_{1-x}\text{Pd}_x)_3$ and show that it ideally qualifies to study pure SOC tuning. Pd is much lighter than Pt (atomic weight 106.42 instead of 195.084) and thus an increase of the Pd content x should sizeably reduce the SOC of the conduction electrons. By contrast, as we will show below, there is minimal μ and J_K tuning involved as the substitution is isoelectronic and the lattice parameter is essentially constant across the substitution series.

Single crystals of $\text{Ce}_3\text{Bi}_4(\text{Pt}_{1-x}\text{Pd}_x)_3$ were grown using a modified Bi flux method (Supplemental Material). The substitution levels x were determined by EDX measurements (Supplemental Material). The lattice parameter a across the sample series is shown in Fig. 1. The accumulated relative change $\Delta a/a(x) = [V(x)/V(x=0)]^{1/3} - 1$, where $V(x)$ denotes the unit cell volume for a given substitution level x , is only 0.069% at $x = 1$. This is extremely small compared to substitutions in related materials. For instance, the substitution of Pt by Cu and Au in $\text{Ce}_3\text{Sb}_4\text{Pt}_3$ results in $\Delta a/a(x=1) = +2.45\%$ and -0.65% , respectively and the substitution of Ni by Pt and Pd in the Kondo semimetal CeNiSn leads to expansions of 2.25% and 1.5%, respectively (Fig. 1). Thus, unlike in these other substitution series, chemical pressure tuning (changing J_K) and charge carrier concentration tuning (changing μ) can be excluded as dominating factors in the $\text{Ce}_3\text{Bi}_4(\text{Pt}_{1-x}\text{Pd}_x)_3$ sample series studied here.

Figure 2 shows the temperature dependence of the electrical resistance, normalized to its room temperature value, of all investigated $\text{Ce}_3\text{Bi}_4(\text{Pt}_{1-x}\text{Pd}_x)_3$ crystals. The resistivity values at 300 K, $\rho_{300\text{K}}$, range between 180 and $350 \mu\Omega\text{cm}$, in good agreement with the published value of $220 \mu\Omega\text{cm}$ for $\text{Ce}_3\text{Bi}_4\text{Pt}_3$ [22]. We expect $\rho_{300\text{K}}$ to be independent of x and attribute the small differences to the poorly defined geometrical factors of the small single crystals.

With increasing x , the resistivity at low temperatures is successively reduced, corresponding to a gradual closing of the Kondo insulator gap (Fig. 2). This can be quantified by Arrhenius fits to the high-temperature data [Fig. 2 (b,c)], which represent a thermally activated resistance described by $R = R_0 \exp[\Delta/(2k_B T)]$, where Δ is the gap width and k_B is the Boltzmann constant. The continuous decrease of Δ with x is shown in Fig. 3. Gap values that are much smaller than the lower boundary

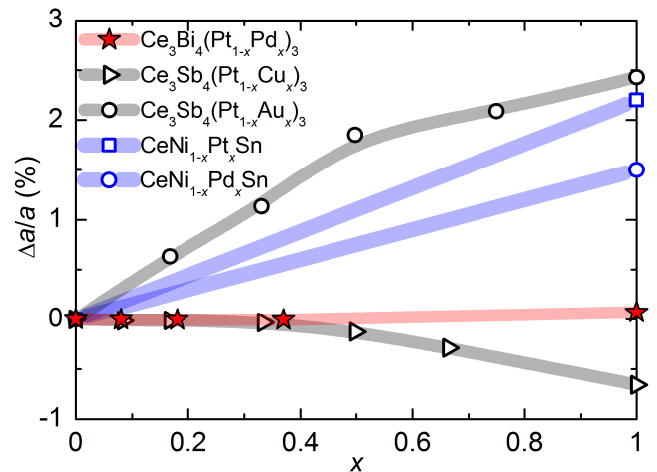


FIG. 1. (Color online) Relative change of lattice parameter a as function of the Pd content x in $\text{Ce}_3\text{Bi}_4(\text{Pt}_{1-x}\text{Pd}_x)_3$ (red), on a scale relevant to other archetypal Kondo systems [29–32] (open symbols). Lines are guides to the eyes.

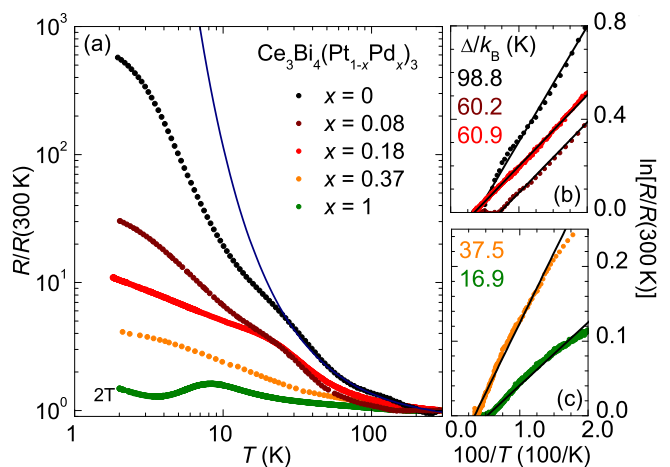


FIG. 2. (Color online) (a) Temperature-dependent electrical resistance $R(T)$, normalized to its room temperature value $R(300\text{K})$, on a log-log scale for all investigated $\text{Ce}_3\text{Bi}_4(\text{Pt}_{1-x}\text{Pd}_x)_3$ samples. An exponentially activated resistivity, fitted to the high-temperature regime of the $x = 0$ sample, is shown as blue line. (b),(c) Arrhenius plots for data above 50 K. The solid lines are the fits (see text). The data for the $x = 1$ sample were taken at 2 T to suppress a spurious superconducting resistance drop at 3 K that had no correspondence in magnetization and specific heat measurements. This magnetic field has no effect on the resistance data above 3 K.

of the fitting range are unphysical. This is the case for the $x = 1$ sample. The energy gap of 16.9 K should thus be taken with caution – and rather as indication for the absence of a well-defined gap in $\text{Ce}_3\text{Bi}_4\text{Pd}_3$. In fact, the resistance of this sample depends only very weakly on temperature, which is characteristic of semimetals. At 8.3 K, a broad local maximum is observed. As will be shown below, this feature is echoed by anomalies in the magnetization (Fig. 4) and specific heat (Fig. 5), and is likely due to Kondo interaction in a semimetal.

The magnetic susceptibility of all investigated

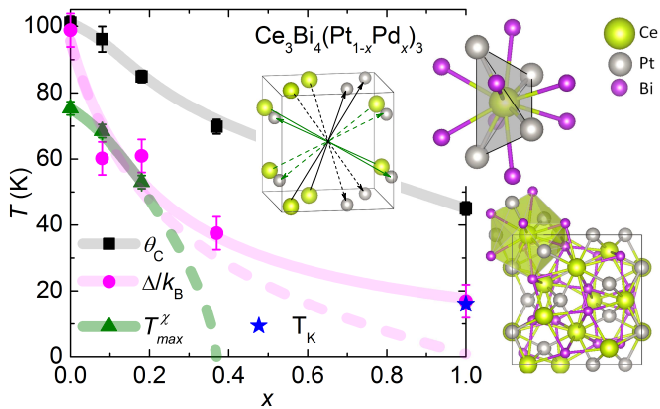


FIG. 3. (Color online) Characteristic temperature scales for $\text{Ce}_3\text{Bi}_4(\text{Pt}_{1-x}\text{Pd}_x)_3$ as function of x . T_{max}^x and Θ_C are taken from Fig. 4(c) and the Curie-Weiss fits in Fig. 4(b), respectively. Δ/k_B is taken from the Arrhenius fits in Fig. 2(b,c). The Kondo temperature T_K is taken from the entropy analysis in Fig. 5(c). The full lines are guides to the eyes. The dashed pink line reflects the fact that for $x = 1$ the Arrhenius fit loses significance (see text). The dashed green line indicates that the maximum in $\chi(T)$ is suppressed to below 2 K for $x = 0.37$. The structure sketches illustrate the unit cell (bottom), the environment of Ce with 4 nearest Pt/Pd (3.01 Å) and 8 next-nearest Bi (3.041 Å) neighbours (top), and the lack of a center of inversion for (selected) Ce and Pt atoms.

$\text{Ce}_3\text{Bi}_4(\text{Pt}_{1-x}\text{Pd}_x)_3$ samples [Fig. 4(a)] is well described by a Curie-Weiss law at high temperatures [Fig. 4(b)]. The effective magnetic moments, obtained by Curie-Weiss fits between 150 and 300 K, all range between 2.5 and 2.6 μ_B , which is close to the value of 2.54 μ_B expected for a free Ce^{3+} ion. This confirms that the Ce ions are in a trivalent state. The paramagnetic Weiss temperature Θ_C , which is negative for all samples, decreases continuously in absolute value from about 100 K for $x = 0$ to 45 K for $x = 1$ (Fig. 3). Θ_C is a measure of the strength of antiferromagnetic (AFM) correlations driven by the Kondo interaction, which thus decrease upon Pd substitution. However, interestingly, Θ_C remains sizeable even for the $x = 1$ sample. This indicates that rather strong AFM correlations remain present up to the end compound $\text{Ce}_3\text{Bi}_4\text{Pd}_3$. This is in sharp contrast to the Au-Pt and Cu-Pt substitutions in $\text{Ce}_3\text{Sb}_4\text{Pt}_3$ which suppress $-\Theta_C$ from 647 K in $\text{Ce}_3\text{Sb}_4\text{Pt}_3$ to less than 3 K and 1 K in $\text{Ce}_3\text{Sb}_4\text{Au}_3$ [32] and $\text{Ce}_3\text{Sb}_4\text{Cu}_3$ [31], respectively.

A maximum in the magnetic susceptibility, as observed at $T_{\text{max}}^x = 75$ K for the $x = 0$ sample [Fig. 4(a,c)] in good agreement with previous findings [22, 24], signals the onset of Kondo screening associated with the opening of the Kondo insulator gap [6]. With increasing x , T_{max}^x is successively suppressed (Fig. 3). The $x = 0.37$ sample shows no maximum down to at least 2 K. The typically observed upturn of the susceptibility at the lowest temperatures, that has no correspondence in neutron scattering experiments [23], is generally attributed to a Curie tail due to a small amount of magnetic impurities.

The magnetic susceptibility of $\text{Ce}_3\text{Bi}_4\text{Pd}_3$ is qualita-

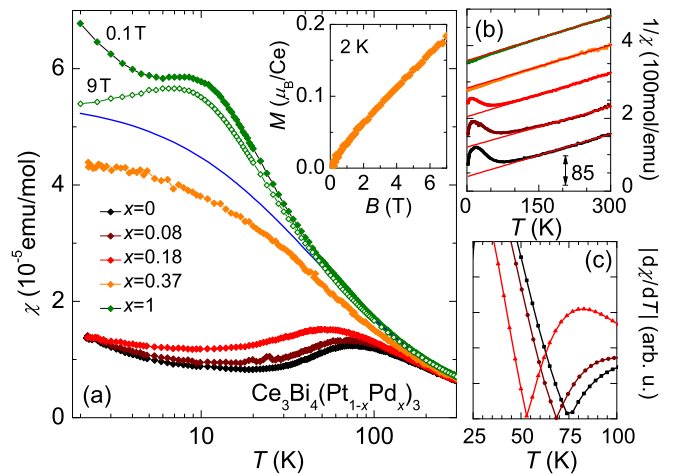


FIG. 4. (Color online) (a) Temperature-dependent magnetic susceptibility $\chi(T)$ of all investigated $\text{Ce}_3\text{Bi}_4(\text{Pt}_{1-x}\text{Pd}_x)_3$ samples, in a magnetic field of 100 mT. Only for the $x = 0.37$ sample a field of 7 T was applied to obtain a good signal. This does not strongly affect the susceptibility in view of the nearly linear-in- B magnetization at 2 K (inset). A Curie-Weiss fit for the $x = 0$ data is also shown (blue). (b) χ^{-1} vs T along with the Curie-Weiss fits that determine the paramagnetic Weiss temperature Θ_C . The data for $x > 0$ are successively shifted by 85 mol Oe/emu for clarity. (c) Absolute value of the temperature derivative $|d\chi/dT|$ vs T for the $x = 0, 0.08$, and 0.18 samples. The sharp minima represent the zero crossings of $d\chi/dT$ and thus the maxima of $\chi(T)$ at T_{max}^x .

tively different. Below 50 K, it deviates to values larger than the Curie-Weiss law [blue line in Fig. 4(a)] and tends to saturate below 10 K, characteristics of heavy fermion metals. The Curie tail at the lowest temperatures is again suppressed by magnetic fields.

Further information on the nature of the ground state of $\text{Ce}_3\text{Bi}_4\text{Pd}_3$ can be extracted from specific heat C_p measurements [Fig. 5(a)]. When plotted as C_p/T vs T^2 , an anomaly can be discerned below 15 K [Fig. 5(b)]. Its background can be modeled by $C_p/T = \gamma + \beta T^2$ where γ is the Sommerfeld coefficient of the electronic contribution and the β term represents the low-temperature Debye approximation for the lattice contribution. The data are consistent with $\gamma = 226$ mJ/(mol-CeK²) and $\beta = 4.39$ mJ/(mol-CeK⁴). The latter corresponds to a Debye temperature Θ_D of 160 K, in good agreement with previous results on both $\text{Ce}_3\text{Bi}_4\text{Pt}_3$ [25] and the nonmagnetic reference compound $\text{La}_3\text{Bi}_4\text{Pt}_3$ [22]. The electronic term γ is much larger than the values of 7 mJ/(mol-CeK²) for $\text{Ce}_3\text{Bi}_4\text{Pt}_3$ in zero field, 20 mJ/(mol-CeK²) for $\text{Ce}_3\text{Bi}_4\text{Pt}_3$ in 60 T, and 9 mJ/(mol-LaK²) for $\text{La}_3\text{Bi}_4\text{Pt}_3$ [25], pointing to the strongly correlated nature of the ground state of $\text{Ce}_3\text{Bi}_4\text{Pd}_3$. This is further corroborated by the large amount of electronic entropy released at low temperatures: 0.4 ln 2 per Ce is reached at 8 K [Fig. 5(c)]. Twice this temperature, thus 16 K, is generally considered as good estimate of the Kondo temperature T_K [14, 35].

Figure 3 summarizes the effects of increasing Pd content x and thus decreasing SOC strength: The (absol-

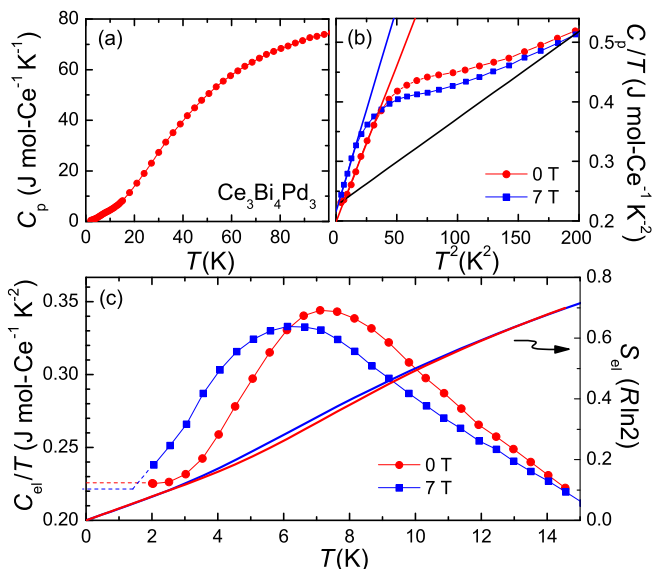


FIG. 5. (Color online) (a) Temperature-dependent specific heat $C_p(T)$ of $Ce_3Bi_4Pd_3$ below 100 K. (b) C_p/T vs T^2 below 15 K, in zero field and in a field of 7 T. The straight lines represent fits described in the text. (c) Electronic specific heat coefficient C_{el}/T in 0 and 7 T (left) and corresponding entropy S_{el} (right) vs temperature. The dashed lines represent the extrapolation to $T = 0$ used to determine the entropy.

lute value of the) paramagnetic Weiss temperature Θ_C decreases with increasing x , but remains sizeable even for $x = 1$. The Kondo insulator gap Δ is reduced with increasing x and cannot be clearly discerned beyond $x = 0.37$. The spin screening temperature T_{max}^x is likewise reduced with x , to below 2 K for $x = 0.37$. For the semimetal $Ce_3Bi_4Pd_3$ at $x = 1$, it reappears in the form of a Kondo temperature of 16 K, as determined from the electronic entropy. Inspecting the crystal structure reveals why the system reacts so sensitively to the Pt-Pd substitution: The Ce atoms have only Pt (Pd) as nearest neighbors, arranged in a tetrahedral environment (Fig. 3 upper right inset). Apparently, the direct overlap of the $5d$ ($4d$) orbitals of Pt (Pd) with the $4f$ orbitals of Ce is a key ingredient for SOC tuning of $Ce_3Bi_4(Pt_{1-x}Pd_x)_3$. Interestingly, imaging Ce at the unit cell center transforms it into Pt (Pd) and vice versa (Fig. 3 left inset).

It is remarkable that the substitution of Bi by the much lighter isoelectronic element Sb has an entirely different effect: Instead of closing the Kondo insulator gap it strongly increases it to 1080 K [32]. This must be due to the smaller size of Sb, that leads to a smaller lattice parameter of 9.82 Å [32], and thus a stronger hybridization, similar to the gap opening under hydrostatic pressure [26].

Finally, we report a discovery that may hint at the nature of the heavy semimetal phase $Ce_3Bi_4Pd_3$ assumes. The low-temperature tail of the specific heat anomaly displays $C_p/T \sim T^2$ behavior, with a slope β' that is sizeably larger than the slope β of the phonon specific heat. Similar behavior was seen in the cubic heavy fermion antiferromagnet $CeIn_3$ below the Néel temperature [36, 37]

and attributed to 3-dimensional (3D) AFM magnons. However, in $Ce_3Bi_4Pd_3$, there is no obvious sign of a magnetic phase transition as the observed anomalies appear too broad to represent such transitions. In addition, a magnetic field of 7 T reduces the maximum of the anomaly only slightly, from 7.1 K to 6 K [Fig. 5(c)]. In view of the linear coupling of a magnetic field to a symmetry breaking order parameter, a stronger suppression would be expected if the anomaly indeed represented AFM ordering. Finally, the magnetic field enhances β' , but would be expected to reduce it in a 3D AFM magnon scenario [38–40].

Instead, we suggest that the $\beta'T^2$ contribution to C_p/T originates from bulk electronic states with linear dispersion $\varepsilon_{\mathbf{k}} = \hbar v^* k$, with the quasiparticle velocity v^* , predicted for a Weyl-Kondo semimetal [12]. Such states contribute a volume specific heat of $7\pi^2/30 \cdot k_B[(k_B T)/(\hbar v^*)]^3$ (Supplemental Materials of [12]). From our experiments we determine $v^* = 886$ m/s which is three orders of magnitude smaller than the Fermi velocity of a simple metal. This agrees well with the Kondo temperature of 16 K (\sim meV) being three orders of magnitude smaller than the Fermi temperature of a simple metal (\sim eV).

Also the experimentally observed evolution from a Kondo insulator phase in $Ce_3Bi_4Pt_3$ to a Weyl-Kondo semimetal phase in $Ce_3Bi_4Pd_3$ that, as detailed above, is due to pure SOC tuning, is in agreement with theoretical expectations: A recent study of the Anderson lattice model in the presence of SOC observed a topological Kondo insulator to Dirac-Kondo semimetal transition as the SOC is decreased [11]. For the case of a noncentrosymmetric crystal structure, the transition is between a topological Kondo insulator and a Weyl-Kondo semimetal [12]. This exciting perspective calls for additional experiments, to further probe the predicted topological bulk and surface states.

Similar SOC tuning studies may also shed light on the topological nature of other strongly correlated semimetals, such as $CeRu_4Sn_6$ [41] and $CeNiSn$ [42], that have been suggested to host topological bulk and/or surface states [27, 43, 44]. In the substitution series $Yb_3(Rh_{1-x}Ir_x)_4Ge_{13}$ a metal to AFM insulator crossover was observed with increasing x [45]. Interestingly, the Rh-Ir substitution is isoelectronic, isostructural, and almost isosize, suggestive of predominant SOC tuning, though this was not acknowledged in that work.

In conclusion we have presented noncentrosymmetric $Ce_3Bi_4(Pt_{1-x}Pd_x)_3$ as a model system for spin-orbit coupling (SOC) tuning of a Kondo insulator. A continuous decrease of the SOC strength is achieved by the isoelectronic, isostructural, and isosize substitution of the heavy element Pt by the much lighter element Pd on the nearest neighbour site of Ce in the crystal structure. The observed Kondo insulator to heavy semimetal transition, with a signature of linearly dispersing quasiparticles of low velocity, can be understood in the context of an Anderson lattice model subject to SOC of varying strength

[11, 12], that predicts a transition between a topological Kondo insulator and a Weyl-Kondo semimetal in the absence of inversion symmetry [12]. We expect these findings to trigger experiments in other strongly correlated materials.

We gratefully acknowledge fruitful discussions with S.

E. Grefe, H.-H. Lai, and E. Morosan, helpful advice from K. Hradil, W. Artner, and D. Joshi and financial support from the Austrian Science Funds (doctoral program W1243 and I2535-N27) and the U.S. Army Research Office (ARO Grant No. W911NF-14-1-0496) in Vienna, and the ARO (Grant No. W911NF-14-1-0525) and the Robert A. Welch Foundation (Grant No. C-1411) at Rice.

-
- [1] See, e.g., Focus Issue “Topological matter”, *Nat. Phys.* **12**, No. 7, pp. 615-718, (2016).
- [2] M. Z. Hasan and C. L. Kane, *Rev. Mod. Phys.* **82**, 3045 (2010).
- [3] X.-L. Qi and S.-C. Zhang, *Rev. Mod. Phys.* **83**, 1057 (2011).
- [4] See, e.g., Focus Issue “Topological semimetals”, *Nat. Mater.* **15**, No. 11, (2016).
- [5] G. Aeppli and Z. Fisk, *Comments Condens. Matter Phys.* **16**, 155 (1992).
- [6] P. S. Riseborough, *Adv. Phys.* **49**, 257 (2000).
- [7] M. Dzero, K. Sun, V. Galitski, and P. Coleman, *Phys. Rev. Lett.* **104**, 106408 (2010).
- [8] V. Alexandrov, M. Dzero, and P. Coleman, *Phys. Rev. Lett.* **111**, 226403 (2013).
- [9] M. Dzero, J. Xia, V. Galitski, and P. Coleman, *Annu. Rev. Condens. Matter Phys.* **7**, 249 (2016).
- [10] X.-Y. Feng, J. Dai, C.-H. Chung, and Q. Si, *Phys. Rev. Lett.* **111**, 016402 (2013).
- [11] X.-Y. Feng, H. Zhong, J. Dai, and Q. Si, Dirac-Kondo semimetals and topological Kondo insulators in the dilute carrier limit, arXiv:1605.02380 (2016).
- [12] H.-H. Lai, S. E. Grefe, S. Paschen, and Q. Si, “Weyl-Kondo semimetal in a heavy fermion system,” arXiv:1612.0000 (2016).
- [13] H. v. Löhneysen, A. Rosch, M. Vojta, and P. Wölfle, *Rev. Mod. Phys.* **79**, 1015 (2007).
- [14] P. Gegenwart, Q. Si, and F. Steglich, *Nature Phys.* **4**, 186 (2008).
- [15] Q. Si and S. Paschen, *Phys. Status Solidi B* **250**, 425 (2013).
- [16] J. W. Allen, R. M. Martin, X. Parc, B. Batlogg, and P. Wachter, *J. Appl. Phys.* **49**, 2078 (1978).
- [17] J. C. Nickerson, R. M. White, K. N. Lee, R. Bachmann, T. H. Geballe, and G. W. Hull, *Phys. Rev. B* **3**, 2030 (1971).
- [18] M. Kasaya, F. Iga, K. Negishi, S. Nakai, and T. Kasuya, *J. Magn. Magn. Mater.* **31-34, Part 1**, 437 (1983).
- [19] M. Okawa, Y. Ishida, M. Takahashi, T. Shimada, F. Iga, T. Takabatake, T. Saitoh, and S. Shin, *Phys. Rev. B* **92**, 161108 (2015).
- [20] Z. Schlesinger, Z. Fisk, H.-T. Zhang, M. B. Maple, J. DiTusa, and G. Aeppli, *Phys. Rev. Lett.* **71**, 1748 (1993).
- [21] S. Paschen, E. Felder, M. A. Chernikov, L. Degiorgi, H. Schwer, H. R. Ott, D. P. Young, J. L. Sarrao, and Z. Fisk, *Phys. Rev. B* **56**, 12916 (1997).
- [22] M. F. Hundley, P. C. Canfield, J. D. Thompson, Z. Fisk, and J. M. Lawrence, *Phys. Rev. B* **42**, 6842 (1990).
- [23] A. Severing, J. D. Thompson, P. C. Canfield, Z. Fisk, and P. Riseborough, *Phys. Rev. B* **44**, 6832 (1991).
- [24] B. Bucher, Z. Schlesinger, P. C. Canfield, and Z. Fisk, *Phys. Rev. Lett.* **72**, 522 (1994).
- [25] M. Jaime, R. Movshovich, G. Stewart, W. Beyermann, M. Berisso, M. Hundley, P. Canfield, and J. Sarrao, *Nature* **405**, 160 (2000).
- [26] J. C. Cooley, M. C. Aronson, and P. C. Canfield, *Phys. Rev. B* **55**, 7533 (1997).
- [27] P.-Y. Chang, O. Erten, and P. Coleman, “Möbius Kondo insulators,” arXiv: 1603.03435v2 (2016).
- [28] K. V. Shanavas, Z. S. Popović, and S. Satpathy, *Phys. Rev. B* **90**, 165108 (2014).
- [29] S. Nishigori, H. Goshima, T. Suzuki, T. Fujita, G. Nakamoto, T. Takabatake, H. Fujii, and J. Sakurai, *Physica B* **186 & 188**, 406 (1993).
- [30] M. Kasaya, T. Tani, F. Iga, and T. Kasuya, *J. Magn. Magn. Mater.* **76**, 278 (1988).
- [31] C. D. W. Jones, K. A. Regan, and F. J. DiSalvo, *Phys. Rev. B* **60**, 5282 (1999).
- [32] K. Katoh and M. Kasaya, *J. Phys. Soc. Jpn.* **65**, 3654 (1996).
- [33] P. Schlottmann, *Phys. Rev. B* **46**, 998 (1992).
- [34] T. Pietrus, H. Löhneysen, and P. Schlottmann, *Phys. Rev. B* **77**, 115134 (2008).
- [35] V. I. Mel’nikov, *JETP Lett.* **35**, 511 (1982).
- [36] A. Berton, J. Chaussy, G. Chouteau, B. Cornut, J. Flouquet, J. Odin, J. Palleau, J. Peyrard, and R. Tournier, *J. Phys. Colloq.* **40**, C5 (1979).
- [37] A. L. Cornelius, P. G. Pagliuso, M. F. Hundley, and J. L. Sarrao, *Phys. Rev. B* **64**, 144411 (2001).
- [38] S. Deonarane and S. J. Joshua, *Phys. Stat. Solidi (b)* **57**, 767 (1973).
- [39] M. B. Maple, N. P. Butch, N. A. Frederick, P.-C. Ho, J. R. Jeffries, T. A. Sayles, T. Yanagisawa, W. M. Yuhasz²⁰²¹, S. Chi, H. J. Kang, J. W. Lynn, P. Dai, S. K. McCall, M. W. McElfresh, M. J. Fluss, Z. Henkie, and A. Pietraszko, *Proc. Natl. Acad. Sci. USA* **103**, 6783 (2006).
- [40] K.-A. Lorenzer, Ph.D. thesis, Vienna University of Technology (2012).
- [41] V. Guritanu, P. Wissgott, T. Weig, H. Winkler, J. Sichelschmidt, M. Scheffler, A. Prokofiev, S. Kimura, T. Iizuka, A. M. Strydom, M. Dressel, F. Steglich, K. Held, and S. Paschen, *Phys. Rev. B* **87**, 115129 (2013).
- [42] U. Stockert, P. Sun, N. Oeschler, F. Steglich, T. Takabatake, P. Coleman, and S. Paschen, *Phys. Rev. Lett.* **117**, 216401 (2016).
- [43] M. Sundermann, F. Strigari, T. Willers, H. Winkler, A. Prokofiev, J. M. Ablett, J. P. Rueff, D. Schmitz, E. Weschke, M. Moretti Sala, A. Al-Zein, A. Tanaka, M. W. Haverkort, D. Kasinathan, L. H. Tjeng, S. Paschen, and A. Severing, *Sci. Rep.* **5**, 17937 (2015).
- [44] Y. Xu, C. Yue, H. Weng, and X. Dai, “Heavy Weyl fermion state in CeRu₄Sn₆,” arXiv: 1608.04602 (2016).
- [45] B. K. Rai, I. W. H. Oswald, J. Y. Chan, and E. Morosan, *Phys. Rev. B* **93**, 035101 (2016).

Supplemental Material of “Tuning spin-orbit coupling in the Kondo insulator $\text{Ce}_3\text{Bi}_4\text{Pt}_3$ by Pd substitution”

I. METHODS

$\text{Ce}_3\text{Bi}_4(\text{Pt}_{1-x}\text{Pd}_x)_3$ single crystals were grown using a modified Bi flux method, described in detail below (Sect. II). Powder X-ray diffraction (XRD) measurements were performed on all grown crystals with a commercial X-ray powder diffractometer (PANalytical XPert Pro MPD), using CuK_α radiation (1.54056 Å). A few mg of representative crystals were selected under an optical microscope, and powdered on a Si single crystal wafer oriented in the [007] crystallographic direction, to avoid any reflection of the substrate. The chemical composition and the Pd substitution levels were determined using energy dispersive X-ray (EDX) and wavelength dispersive X-ray (WDX) spectroscopy setups mounted on a commercial scanning electron microscope (SEM: Philips XL-30, EDX: EDAX New XL-20 135-10 UTW+detector, WDX: Microspec WDX-600). The electrical resistivity of the samples was measured using the standard 4-point method, and contacts were made using conductive silver paint. The samples with $x = 0$ and 0.08 were measured in a Quantum Design PPMS, the samples with $x = 0.18, 0.37$, and 1 were measured in a standard ^4He flow cryostat, using a lock-in amplifier with an excitation of $100 \mu\text{A}$ at a frequency of 33.864 Hz. Crystals with similar shape and size were measured. The magnetic susceptibility was measured using a commercial Oxford DC SQUID magnetometer at 100 mT and a Quantum Design PPMS VSM option for the $x = 1$ sample. For the $x = 0.37$ crystal, a field of 7 T was applied. The magnetic property measurements were performed on the same crystals selected for the resistivity measurements, except for $x = 1$, where 14 crystals were measured simultaneously, both at 100 mT and 9 T. Specific heat measurements in zero field and at 7 T for the $x = 1$ sample were done in a Quantum design PPMS system using the thermal relaxation method. To enhance the resolution, 14 representative crystals were selected to perform the measurement.

II. CRYSTAL GROWTH

Five $\text{Ce}_3\text{Bi}_4(\text{Pt}_{1-x}\text{Pd}_x)_3$ crystals with the nominal substitution levels $x_n = 0, 0.1, 0.15, 0.3$, and 1 were grown using the Bi flux technique [1]. The actual substitution levels x

where determined by EDX measurements, as described below (Sect. III). For $x_n = 0$ and 0.1, elementary Ce, Pt, Pd, and Bi in an atomic ratio of $1 : 1 - x_n : x_n : 7$, respectively, were placed in an alumina crucible, and heated to 1100°C in a vacuum sealed quartz tube, using a box furnace. The melt was then slowly cooled to 600°C with a cooling rate of $1^\circ\text{C}/\text{h}$ and left annealing for 12 h. Crystals of typically 1 mm diameter were then extracted from the melt using a centrifuge. We found that this method is not adequate for growing the Pd substituted crystals with $x > 0.1$, as therein the primary stable phase at Bi excess is CeBi_2Pd [2]. For Pd substituted samples with $x > 0.1$, a premelt of $\text{CePt}_{1-x}\text{Pd}_x$ was prepared by melting a stoichiometric amount of the elementary materials in an RF induction furnace under Ar atmosphere. The premelt was then placed in an alumina crucible with Bi in a vacuum sealed quartz tube, and the same heat treatment and growth rates were applied as in case of $x = 0$. We found that the ratio Ce:Pt:Bi of $1 : 1 - x_n : 1.5$ is the optimum to grow Pd substituted crystals. This optimum ratio comes from the interplay of two effects: A smaller content of Bi results in an increased melting temperature of the compound and a quick depletion of the Bi flux (as it is already close to the stoichiometric ratio of $1 : 1 : 1.33$ of the Pd free material), thus impeding the growth of the crystals. However, if the Bi content is higher, a considerable amount of CeBi_2Pd is detected in the XRD diffractogram. The unavoidable quick depletion of the Bi flux limits the size of the grown crystals to diameters of about $300\ \mu\text{m}$.

III. STRUCTURAL AND CHEMICAL ANALYSES

The $\text{Ce}_3\text{Bi}_4(\text{Pt}_{1-x}\text{Pd}_x)_3$ compounds crystallize in the cubic $\text{Y}_3\text{Sb}_4\text{Au}_3$ phase of space group $I\bar{4}3d$, as evidenced by the powder XRD measurements (Fig. 1). The unit cell ($a = 10.051\ \text{\AA}$ for $\text{Ce}_3\text{Bi}_4\text{Pt}_3$, $a = 10.058\ \text{\AA}$ for $\text{Ce}_3\text{Bi}_4\text{Pd}_3$) contains 4 formula units. Thus, 40 atoms make up the rather complicated structure. To better capture it, the local environment of the Ce atom – which is most essential in shaping the extraordinary physical properties of the compound – is presented in its position in the unit cell (lower right inset of Fig. 3, main text) and alone, emphasizing the Pt positions (upper right inset of Fig. 3, main text). Each Ce atom is surrounded by 12 atoms (4 Pt/Pd and 8 Bi). However, Ce has only Pd/Pt atoms as nearest neighbours at $3.01\ \text{\AA}$ distance, arranged in a tetrahedral configuration. The second nearest neighbours are formed by 8 Bi atoms in a distorted polyhedral structure, at a distance

of 3.41 Å. The crystal structure and peak positions deduced from the XRD diffractograms for $x = 0$ and 1 are in good agreement with the previously reported structures of $\text{Ce}_3\text{Bi}_4\text{Pt}_3$ [3] and $\text{Ce}_3\text{Bi}_4\text{Pd}_3$ [4], respectively. The diffraction patterns for $0 \geq x > 1$ show a minor Bi peak, that is due to incomplete centrifuging.

EDX results are presented in Fig. 2 in the range of 0.5 keV to 3.5 keV where the strongest Pt- M , Bi- M , and Pd- L peaks are located at 2 keV, 2.5 keV, and 2.9 keV, respectively. The Pd substitution levels were determined from these spectra. They follow the trend of the nominal substitution levels [Fig. 2(a, inset)]. For unsubstituted $\text{Ce}_3\text{Bi}_4\text{Pt}_3$, the Pt- M peak is comparable in height with the Bi- M peak, whereas the Pd- L lines are absent [Fig. 2(a), black curve]. With increasing Pd substitution, the height of the Pt- M peak successively decreases, and that of the Pd- L peaks increases, while the sum of the atomic contents is unchanged [Fig. 2(a) inset]. This proves that Pd indeed substitutes Pt at the Pt sites of $\text{Ce}_3\text{Bi}_4\text{Pt}_3$, and does not form a separate phase. An SEM image of a selected crystal with $x = 0.37$ [Fig. 2(b)] shows that the substitution is homogeneous and that no secondary phases are present on the sample surface. For the $x = 0.08$ sample, the nominal total Pd atomic content is 2.4 at%, which is comparable to the lower detection limit of the EDX technique. To improve the detection limit, the crystal was also investigated by WDX spectroscopy, which has a better energy resolution, and confirms the presence of a small amount of Pd in the $x = 0.08$ sample [Fig. 2(c)].

-
- [1] P. C. Canfield and Z. Fisk, *Philos. Mag. B* **65**, 1117 (1992).
 - [2] F. Han, X. Wan, D. Phelan, C. C. Stoumpos, M. Sturza, C. D. Malliakas, Q. Li, T.-H. Han, Q. Zhao, D. Y. Chung, and M. G. Kanatzidis, *Phys. Rev. B* **92**, 045112 (2015).
 - [3] M. F. Hundley, P. C. Canfield, J. D. Thompson, Z. Fisk, and J. M. Lawrence, *Phys. Rev. B* **42**, 6842 (1990).
 - [4] W. Hermes, S. Linsinger, R. Mishra, and R. Pöttgen, *Monatsh. Chem.* **139**, 1143 (2008).

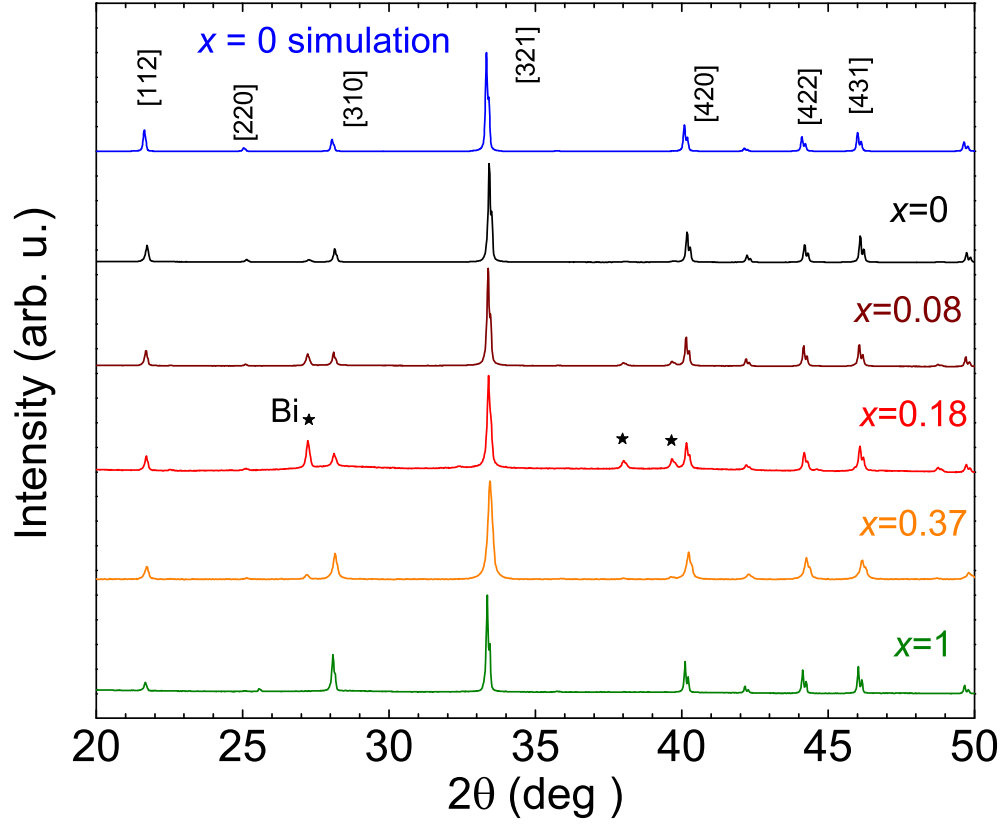


FIG. 1. (Color online) Powder XRD patterns of all investigated batches. The Miller indices and XRD simulation of $\text{Ce}_3\text{Bi}_4\text{Pt}_3$ are also shown. Minor peaks from remaining Bi flux are observed and indicated by stars. They are absent in $\text{Ce}_3\text{Bi}_4\text{Pd}_3$.

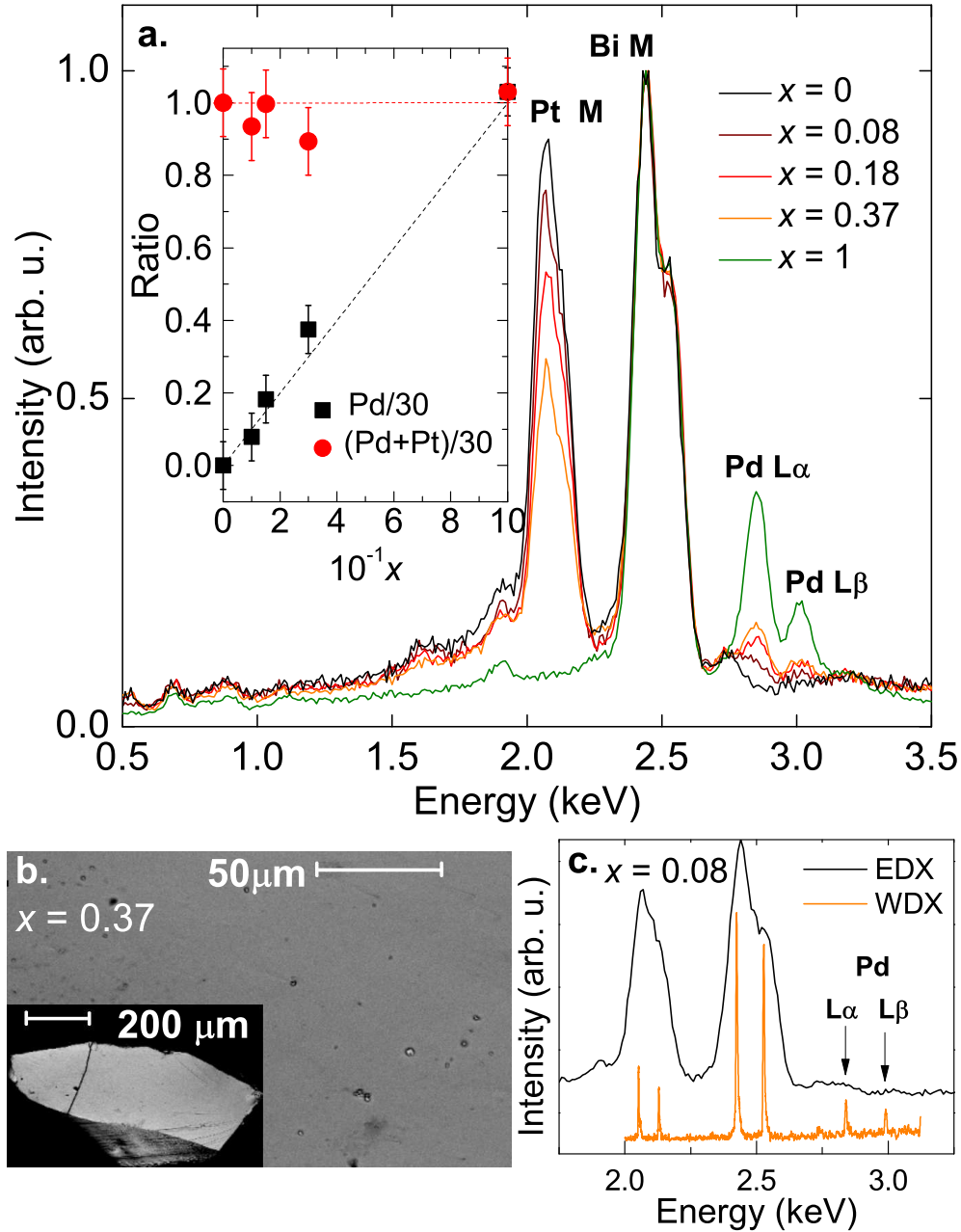


FIG. 2. (Color online) SEM, EDX, and WDX study of $\text{Ce}_3\text{Bi}_4(\text{Pt}_{1-x}\text{Pd}_x)_3$. (a) Variation of the EDX spectra as function of the substitution level (normalized to the Bi-M peak). The inset shows the Pd content along with the Pd+Pt content as compared to the nominal values (dashed lines). (b) Representative SEM image of a $x = 0.37$ sample. (c) WDX spectrum of the $x = 0.08$ sample with clearly resolved Pd peaks.